Experiments and Modeling of Flow-Enhanced Nucleation in LLDPE

THE JOURNAL OF PHYSICAL CHEMISTRY B
A JOURNAL OF THE AMERICAN CHEMICAL SOCIETY

pubs.acs.org/JPCB

Article

Experiments and Modeling of Flow-Enhanced Nucleation in LLDPE

Published as part of The Journal of Physical Chemistry virtual special issue "Doros N. Theodorou Festschrift".

David A. Nicholson, Marat Andreev, Kenneth L. Kearns, Marius Chyasnavichyus, Daria Monaenkova, Jonathan Moore, Jaap den Doelder, and Gregory C. Rutledge*

Cite This: *J. Phys. Chem. B* 2022, 126, 6529–6535

Read Online

ACCESS | Metrics & More | Article Recommendations | Supporting Information

ABSTRACT: A computational and experimental framework for quantifying flow-enhanced nucleation (FEN) in polymers is presented and demonstrated for an industrial-grade linear low-density polyethylene (LLDPE). Experimentally, kinetic measurements of isothermal crystallization were performed by using fast-scanning calorimetry (FSC) for melts that were presheared at various strain rates. The effect of shear on the average conformation tensor of the melt was modeled with the discrete slip-link model (DSM). The conformation tensor was then related to the acceleration in nucleation kinetics by using an expression previously validated with nonequilibrium molecular dynamics (NEMD). The expression is based on the nematic order tensor of Kuhn segments, which can be obtained from the conformation tensor of entanglement strands. The single adjustable parameter of the model was determined by fitting to the experimental FSC data. This expression accurately describes FEN for the LLDPE, representing a significant advancement toward the development of a fully integrated processing model for crystallizable polymers.

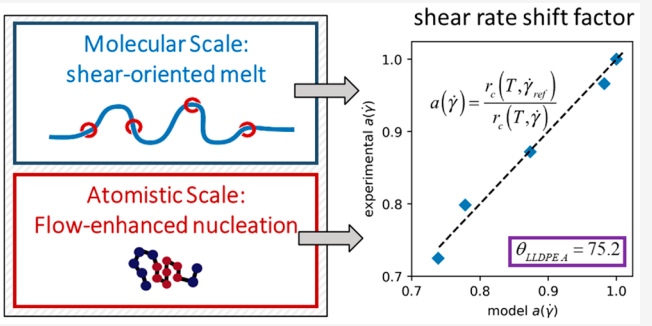

1. INTRODUCTION

When a polymer melt is processed, it is typically subjected to a strong flow field that stretches and orients its constituent chains. For crystallizable polymers, this chain deformation leads to a dramatic acceleration in the crystallization rate through a phenomenon known as flow-induced crystallization (FIC).[1−4] As the intensity of the flow field increases, flow-enhanced nucleation (FEN) occurs, which is characterized by an increase in the nucleation rate of spherulites.[5,6] As a result of FEN, finer-grained semicrystalline morphologies are formed, often leading to enhanced properties. Further increases in the intensity of flow lead to the formation of row-nucleated structures and fibrillar morphologies.[7,8] The formation of these morphologies is accompanied by an acceleration of the growth rate in the flow direction, but the mechanism behind the nucleation event that leads to fibrillar morphologies, and whether it differs from the spherulitic one, is not certain.

Experimentally, a variety of methods have been used to induce flow and measure the acceleration of crystallization kinetics.[1,4] One popular approach is the two-step protocol developed by Janeschitz-Kriegl and co-workers,[9,10] wherein a strain pulse is applied to the melt at a temperature where nucleation can occur, but growth is slow. After the strain pulse, a quench is performed and the development of structure through growth of the crystal nuclei is monitored. This method was designed to separate temporally the processes of nucleation and growth, and it was found to work well for some polymers, in particular isotactic polypropylene (iPP); however, applications of this method to faster crystallizing materials like polyethylene (PE) are not known to the authors. A variation on this method was recently developed by Rhoades et al.[11] in which the strain pulse was applied to the melt at high temperature, followed by a rapid deep quench to freeze in any melt deformation or precursor formation that occurred due to flow. The sample was then microtomed, and fast-scanning calorimetry was performed to measure the isothermal crystallization kinetics. Using rapid annealing cycles, one could study a range of temperatures, without erasing the deformation history within the sample. Originally, this method was used to study the crystallization of poly(ether ether ketone) (PEEK), but this method has also been used to study polyamide nanocomposites[12] and linear low-density polyethylene (LLDPE),[13] which is a rapidly crystallizing polymer.

To interpret the results of flow experiments, it is often necessary to use a rheological model to characterize the response of the melt to the applied flow field. A number of models for viscoelastic fluids have been used in previous

Received: May 18, 2022
Revised: July 23, 2022
Published: August 23, 2022

https://doi.org/10.1021/acs.jpcb.2c03460
J. Phys. Chem. B 2022, 126, 6529−6535

studies, including the multimode Maxwell model,[14] the Giesekus model,[15] the Leonov model,[16] the Doi−Edwards model,[17] the extended Pom-Pom model,[5] the GLaMM model,[18] and the Rolie-Double-Poly model.[19] These models are not easily extended to model melts undergoing crystallization, and with the exception of the Rolie-Double-Poly model, they are only applicable to monodisperse melts. To study polydisperse materials, the discrete slip-link model (DSM)[20] is an attractive alternative to the foregoing models, and supports a future goal of incorporating the work herein with the effect of crystallization on rheology. The DSM is a single-chain model representing entanglements with other chains as slip-links. The slip-link is a constraint on the motion of the chain, but through which chain segments can slide, resulting in reptation-like motion for the chain on longer time scales. The DSM can describe strong flows, melts with varying polydispersity, and the effects of partial crystallinity.[21−25]

Because of the small spatiotemporal scale at which it occurs, FEN is difficult to study experimentally. Consequentially, many researchers have turned to computational methods to glean insight into how FEN occurs and how models should be constructed to include its effect.[3,26,27] In particular, a recent nonequilibrium molecular dynamics (NEMD) study revealed strong correlations between Kuhn segment orientation and nucleation kinetics.[28] Similar conjectures have been made in the past, based on an observed correlation between FEN and the deformation of entanglement strands, which necessarily involves the reorientation of Kuhn segments.[8] The observed correlations were found to be consistent with the coarse-grained model of FEN from Graham and Olmsted and have been utilized in the PolySTRAND continuum model for FEN in polydisperse melts.[18,19] Moreover, recent molecular simulations have shown the importance of Kuhn segment orientation to the formation of precursors to nucleation[29] and the development of flow-induced inhomogeneity.[30]

Despite a great deal of research, the development of processing models for crystallizable polymers lags behind that for their amorphous counterparts.[4] There are a number of factors that contribute to this shortcoming, but a major factor is the absence of universally accepted models that account for both the kinetics of FIC and the rheology of melts undergoing crystallization.[1,28] In this work, we present a model for FEN that uses a rheological model to relate flow to molecular conformation, correlations from atomistic molecular dynamics simulation to relate conformation to nucleation kinetics, and experimental data to determine the single material-dependent enhancement parameter. The framework is demonstrated by using an industrial-grade LLDPE resin. Combined with a recently developed rheological model for crystallizing melts by Andreev et al.,[21,22] this work closes the loop on the two-way coupling between flow dynamics and crystallization kinetics in polymer melts and thus represents an important advancement in the development of processing models for crystallizable polymers.

2. EXPERIMENTAL SECTION

2.1. Material Characterization. The resin used in this study, termed LLDPE A, was provided by Dow, Inc. It is an ethylene−hexene copolymer with a comonomer content of 16 per 1000 C. It is polydisperse with index $Đ = 2.13$, defined as the ratio of the weight-average molar mass (98.5 kDa) to the number-average molar mass (46.2 kDa). The full molecular weight distribution determined by gel permeation chromatography is shown in Figure 1. The dynamic modulus for this material was measured by small-amplitude oscillatory shear (SAOS) in a previous study.[22]

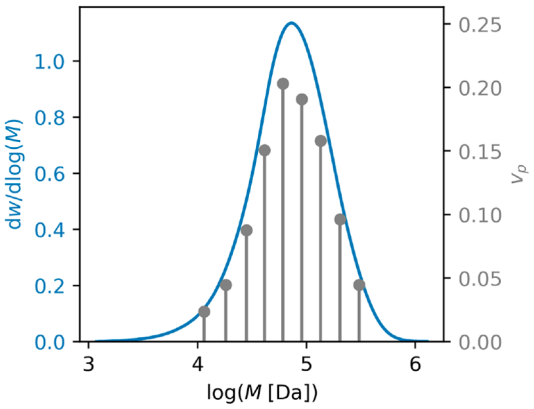

Figure 1. Molecular weight distribution of LLDPE A. The blue curve, which corresponds to the left axis, is the distribution measured by gel-permeation chromatography. The gray marked lines, which correspond to the right axis, are the discretized molecular weights and volume fractions, v_p, used in the slip-link model.

2.2. Rheometry and Sample Preparation. Shear was applied to the sample by using a TA Instruments ARES-G2 strain-controlled rheometer with an 8 mm stainless steel cone-and-plate fixture. For each shear rate, a single LLDPE pellet was melted at 150 °C and then cooled and equilibrated at 120 °C under a nitrogen flow. At this temperature the sample was trimmed, the plates were brought to the measurement gap, and then a flow measurement was performed at 0.1 s^{-1} shear rate for 20 s to ensure consistent rheological properties from sample to sample. Subsequently, the sample was held for a 120 s waiting period and then sheared at a constant strain rate in the range 1−20 s^{-1} for 4 s. After the cessation of shear, the sample was immediately cooled to room temperature according to the fixture thermocouple reading within a few tens of seconds by using a strong airflow from an air gun pointed directly at the sample. Upon cooling, sample disks did not adhere strongly to the fixtures and could be easily detached. Thin ∼12 μm sample sections were then extracted with cryo-microtomy at a single radial position in linear segments perpendicular to the radius of the disc. Polarized optical microscopy was performed on sections taken along the radial direction; the uniformity of the sample morphology from the center to the edge of the plate was confirmed. These samples were then cut and placed on chips for examination by fast scanning calorimetry.

2.3. Fast Scanning Calorimetry (FSC). FSC measurements were performed by using a Mettler Toledo Flash DSC 1 chip calorimeter with UFS 1 chips. Isothermal crystallization measurements were performed by using the procedure described in Kearns et al.[13] Briefly, each sample was first melted at 105 °C for 0.2 s, then cooled at 2000 °C/s to a crystallization temperature between 70 and 85 °C, and held for 2 s to allow crystallization to proceed. Subsequently, the sample was cooled to −95 °C, held for 0.2 s, and then remelted at 105 °C for 0.2 s. From there, the sample was quenched to the next crystallization temperature. This cycle was repeated to obtain crystallization kinetics over the entire temperature range. After isothermal crystallization measurements were

https://doi.org/10.1021/acs.jpcb.2c03460
J. Phys. Chem. B 2022, 126, 6529−6535

obtained over the entire temperature range, an additional measurement was performed at the first crystallization temperature, in this case 70 °C, to confirm that the thermal cycling had no discernible impact on the measured crystallization kinetics. Although the temperature of 105 °C that was used to melt samples is well below the equilibrium melting temperature for PE, complete melting of this material was observed to occur upon heating this material to 105 °C at a scan rate of 1000 °C/s (see Figure S1).

3. MODELS

3.1. Flow-Enhanced Nucleation Model. Although the experimental system is not amenable to study directly by molecular simulation due to the large length and time scales involved, the FEN model draws on correlations that were found by using simulation methods. In particular, a recent atomistic simulation study of $C_{150}H_{302}$ found that the crystal nucleation rate correlated most closely with the degree to which Kuhn segments are oriented, for both shear and extensional flow fields.[28] This orientation was quantified based on invariants of the nematic order tensor of Kuhn segments, $\mathbf{P}_2$. Similar FEN expressions were obtained by using two invariants of $\mathbf{P}_2$: the largest eigenvalue P_2 and the second invariant $J_2(\mathbf{P}_2) = \mathrm{tr}(\mathbf{P}_2^2)$.[28] Either quantity would likely work for the shear protocol described here given that FEN expressions of similar accuracy were obtained by using P_2 and $J_2(\mathbf{P}_2)$ in molecular simulations. The second invariant was chosen since it is more readily generalized to other flow fields that may have multiple orientation directions (e.g., biaxial flow).

It is not always possible to measure experimentally the orientation of Kuhn segments. However, $\mathbf{P}_2$ can be approximated based on the conformation tensor of entanglement strands, $\mathbf{C}$, which is a component of many rheological models. In this work, the relationship from Kuhn and Grün[31,32] was used:

$$\mathbf{P}_2 = \frac{9}{10N_K}\left(\mathbf{C} - \mathbf{I}\frac{\mathrm{tr}(\mathbf{C})}{3}\right) \quad (1)$$

wherein N_K is the number of Kuhn segments per entanglement strand. For polyethylene, the entanglement strand size has been reported to range from 60 to 90 backbone carbons,[33−36] and the Kuhn segment size corresponds to 12.5 backbone carbons.[37] Taking the middle of the range for the entanglement strand size, the value $N_K = 6$ is adopted herein. This expression is valid for small extensions, where the stress-optical rule is expected to hold. On the basis of this relationship, simulation-derived expressions can be used to model the dependence of the nucleation rate, $I(T,\dot{\gamma})$, on $\mathbf{P}_2$ taken directly from molecular simulation results. The FEN expression is as follows:[28]

$$I(T, \dot{\gamma}) = I_q(T)\exp[\theta\sqrt{J_2(\mathbf{P}_2)}] \quad (2)$$

In this expression, $I_q(T)$ is the quiescent nucleation rate and θ is the flow-enhancement parameter.

In polydisperse melts, the longest chains are believed to contribute disproportionately to the FEN rate. To account for this effect, the nucleation rate was averaged over multiple molar mass modes. For each mode p, the nematic order tensor $\mathbf{P}_{2,p}$ was calculated, and its contribution to the nucleation rate was weighted by its volume fraction, ν_p. For a total of P modes, the following FEN expression is obtained:

$$I(T, \dot{\gamma}) = I_q(T)\sum_{p=1}^{P}\nu_p\exp[\theta\sqrt{J_2(\mathbf{P}_{2,p})}] \quad (3)$$

3.2. Slip-Link Model. In the DSM, the dynamics of entangled polymer chains are modeled at the entanglement relaxation time scale. The highly coarse-grained nature of this mesoscale model allows for capture of the long relaxation times associated with the entanglement dynamics of industrial-grade polymers, which can be on the order of seconds.[38] Because the DSM is a single-chain model, its primary relaxation mechanism is the sliding dynamics (SD) of a probe chain through a set of slip-links, which represent entanglements between the probe chain and surrounding chains in the background. The DSM also accounts for constraint dynamics (CD), whereby slip-links relax due to the dynamics of the background chains. DSM calculations are typically performed for an ensemble of probe chains, and macroscopic properties are computed as ensemble averages. The probe chains in such calculations can be selected to represent different molar mass modes. The polydispersity of the background chains is taken into account by including additional relaxation times for CD.[24,25] Because of its ability to account for polydispersity, the DSM is a good method for studying polydisperse polymer melts like the LLDPE considered herein. Importantly, a version of the DSM that includes modes associated with polydisperse dangling and bridging chain segments has been shown elsewhere to capture the effect of crystallization on rheology in the absence of flow for the same LLDPE studied here.[22] Given that no notable crystallization occurs during flow in this study, these additional modes were not necessary; nevertheless, the selection of the DSM as the rheological model in this work was made in anticipation of combining the two approaches in the near future to obtain a fully integrated FIC model.

A parametrization of a DSM for LLDPE was reported in a prior study;[22] however, adjustments were made herein to more accurately reproduce the molecular weight distribution and account for discrepancies in the transient viscosity data between different experimental setups. These types of discrepancies are common when comparing data from different experiments. For example, a time discrepancy may be due to differences in temperature control, whereas a stress discrepancy may be due to differences in geometry and loading. In this case, a model was first fit based on the small-amplitude oscillatory shear data reported previously,[22] and the time scale was subsequently adjusted to match transient viscosity results reported in Figure 2.

The slip-link model parameters are the average molecular weight of an entanglement strand, $M_e = 1100$ Da, and the time scale associated with sliding dynamics, $\tau_K(T = 107\ °C) = 0.027$ μs, based on SAOS data. The representation of polydispersity was also the same as that used in the previous study.[22] Briefly, the approach of Valadez-Pérez et al.[39] was used, in which background chains are represented by many molar mass modes (161 in this case), while probe chains are represented by a small number of molar mass modes ($P = 9$ in this case). The probe chain modes used and their volume fractions, ν_p, are shown in Figure 1. The number of probe chain modes was determined from the quality of linear viscoelastic (LVE) fit, without consideration of flow calculations. For each probe chain mode, an ensemble of $N_{c,p} = 25$ chains was simulated, for a grand total of 225 chains. For flow calculations, the probe

https://doi.org/10.1021/acs.jpcb.2c03460
J. Phys. Chem. B 2022, 126, 6529−6535

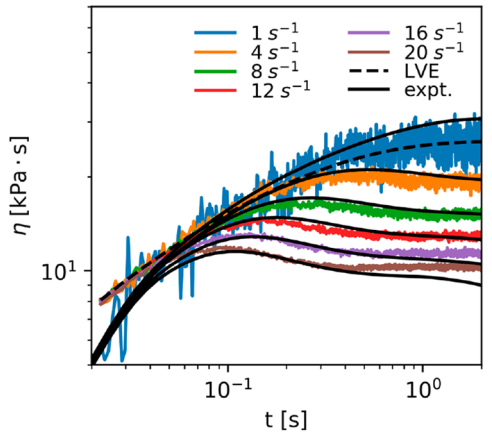

Figure 2. Transient viscosity during start-up shear of LLDPE A at 120 °C. The solid, colored lines are DSM calculations at various strain rates. The dashed black line is the linear viscoelastic envelope (LVE) from the DSM. The solid black lines are experimental data. As is described in the text, the DSM and LVE data were shifted to match the experimental LVE at small time and low strain rate.

chain ensemble was increased to $N_{c,p}$ = 4000 for the four largest molar mass modes, to improve signal to noise.

Start-up flow calculations were performed in the DSM by deforming the positions of slip-links affinely at every time step. This deformation operation increases the computational cost of the DSM; however, the DSM can be massively parallelized by implementation on GPUs, offsetting the increased number in arithmetic operations. The time scale τ_K was adjusted to 0.0522 μs to improve the model fit to the transient viscosity data. A comparison of the DSM calculations and the rheometric data is shown in Figure 2. At 120 °C, the molecular weight-averaged relaxation time of the melt is 0.15 s, and the relaxation time of the largest molar mass mode, 300 kDa, is 1.42 s. The largest molar mass mode corresponds to 4.3% of the melt by volume.

For probe chain mode p, the conformation tensor was calculated from slip-link model chain conformations via the following expression:

$$\mathbf{C}_p = \left\langle \sum_{i=1}^{Z_k} \frac{\mathbf{Q}_{i,k}\mathbf{Q}_{i,k}}{N_{i,k}} \frac{N_{i,k}}{N_{s,p}} \right\rangle_{k=1,\ldots,N_{c,p}} = \left\langle \sum_{i=1}^{Z_k} \frac{\mathbf{Q}_{i,k}\mathbf{Q}_{i,k}}{N_{s,p}} \right\rangle_{k=1,\ldots,N_{c,p}} \quad (4)$$

In eq 4, $\langle \ldots \rangle$ denotes an average over all of the chains in mode p, $\mathbf{Q}_{i,k}$ is the ith slip-link connector vector for chain k, $N_{i,k}$ is the number of chain segments on the ith slip-link connector vector for chain k, Z_k is the number of entangled strands on chain k, and $N_{s,p}$ is the total number of segments for a chain in mode p. In eq 4, the conformation tensor for a strand, $\mathbf{Q}_{i,k}\mathbf{Q}_{i,k}/N_{i,k}$, is weighted by the fraction of the chain's segments that it contains, $N_{i,k}/N_{s,p}$. This weighted average takes into account the fluctuating number of entanglements as well as the fluctuating number of chain segments between slip-links in the DSM.

4. RESULTS AND DISCUSSION

For each shear rate, the crystallization rate was measured experimentally over the temperature range 70−85 °C in increments of 1 °C by using FSC. The crystallization rate, r_c, was taken as the inverse of the peak time. The crystallization rate curves are shown in Figure 3a. The data at 80−85 °C were omitted and not considered for further analysis due to large observed variances in the crystallization rates at these temperatures. At each strain rate, the crystallization rate increases with decreasing temperature, which is an indication that crystallization is occurring within a nucleation-limited regime.[40] On the basis of the experimental protocol, in which the melt is presheared at high temperature and then FIC is measured at lower temperatures in the absence of flow, the growth rate, G, is not expected to be sensitive to the flow. For similar systems, e.g., polypropylene, in which preshearing was followed by crystallization, no notable dependence of the spherulitic growth rate on the strain rate was observed.[5,14] Additionally, polarized optical micrographs confirm that higher shear rates lead to a finer grained structure (see Figure S2), which is consistent with nucleation rate being most affected by flow. As a result, the overall crystallization rate for spontaneous nucleation and three-dimensional growth, $r_c \propto (IG^3)^{1/4}$, is assumed to have a form similar to eq 3:

$$r_c(T, \dot{\gamma}) = r_{c,q}(T)\left(\sum_{p=1}^{P} \nu_p \exp[\theta\sqrt{J_2(\mathbf{P}_{2,p})}]\right)^{1/4} \quad (5)$$

In this expression, $r_{c,q}(T)$ is the quiescent crystallization rate.

In eq 5, the temperature dependence of the flow-induced crystallization rate comes only from the quiescent rate

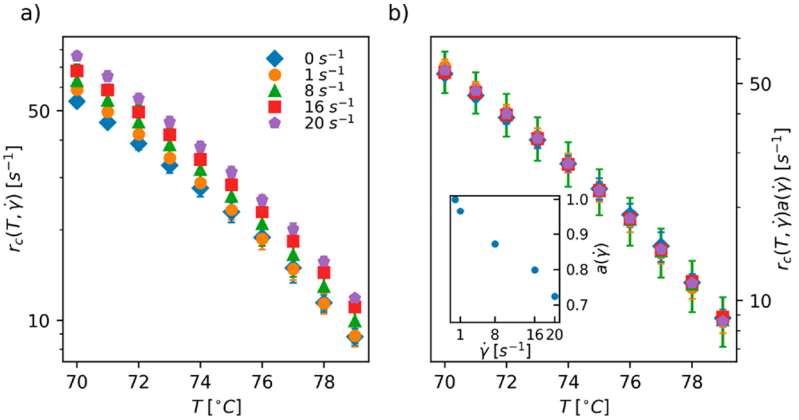

Figure 3. (a) FSC measurements of the isothermal crystallization rate at each shear rate for a range of temperatures. (b) Crystallization rates modified by the shift factors, $a(\dot{\gamma})$, shown in the inset. The error bars denote the standard deviation across three measurements.

https://doi.org/10.1021/acs.jpcb.2c03460
J. Phys. Chem. B 2022, 126, 6529−6535

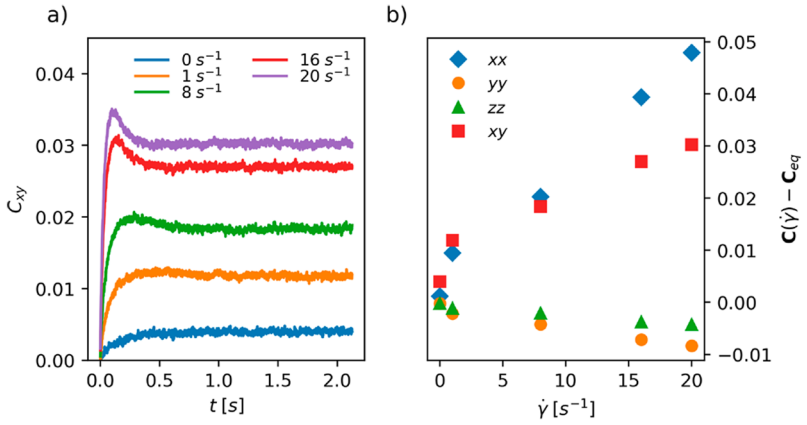

Figure 4. Behavior of the conformation tensor for LLDPE A during DSM simulations: (a) the *xy* component of the conformation tensor for start-up shear; (b) the steady-state values of the deviation of the nonzero components of the conformation tensor from equilibrium for each strain rate.

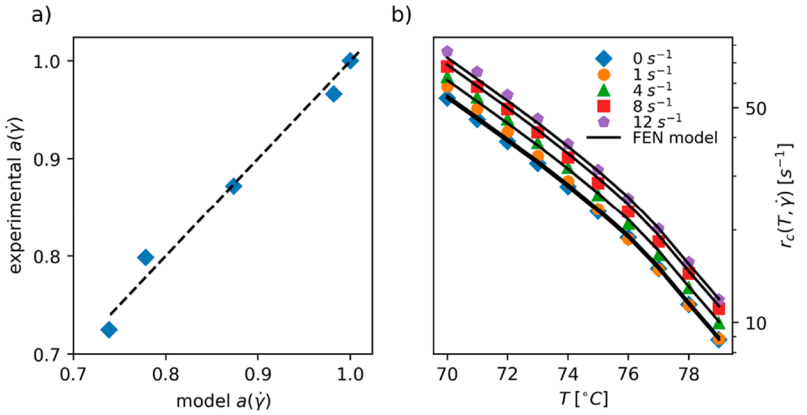

Figure 5. (a) Relationship between experimental values of $a(\dot{\gamma})$ and the fit to the model expression in eq 9. The line corresponds to $y = x$. (b) FSC crystallization rates shown in Figure 3 along with the results using the model expression in eq 5.

behavior. Therefore, for two distinct strain rates $\dot{\gamma}'$ and $\dot{\gamma}''$, we introduce the concept of a shear rate shift factor $a(\dot{\gamma})$ such that $r_c(T,\dot{\gamma}')a(\dot{\gamma}') = r_c(T,\dot{\gamma}'')r_c(T,\dot{\gamma}'')$. Defining $a(\dot{\gamma}_r) = 1$ for a reference shear rate $\dot{\gamma}_r$, the $r_c(T,\dot{\gamma})$ curves at the remaining shear rates can be shifted vertically to overlap as closely as possible with the crystallization rate at $\dot{\gamma}_r$, resulting in the following shear rate shift factors:

$$a(\dot{\gamma}) = \frac{r_c(T, \dot{\gamma}_r)}{r_c(T, \dot{\gamma})} \tag{6}$$

In this study, the quiescent melt was chosen as the reference strain rate, $\dot{\gamma}_r = 0$, and the shift factors were determined by minimizing the following objective function at each strain rate:

$$f[a(\dot{\gamma})] = (\log[r_c(T, \dot{\gamma})a(\dot{\gamma})] - \log[r_c(T, \dot{\gamma}_r)])^2 \tag{7}$$

The adjusted $r_c(T,\dot{\gamma})$ curves and the resulting shift factors are shown in Figure 3b. The nearly overlapping points at each temperature suggest that the temperature dependence in eq 5 holds well for this material. The values of $a(\dot{\gamma})$, shown in the inset of Figure 3b, indicate a steady increase in the crystallization rate with shear rate over the studied range of 1−20 s^{-1}. Although it was not the case in this study, in the event that quiescent crystallization data are not available or easily obtained, the method could still be used with a different choice of $\dot{\gamma}_r$. Furthermore, an accurate quiescent crystallization model could serve in place of experimental data for $r_{c,q}(T)$.

Flow calculations were performed by using the DSM for each shear rate to compute the conformation tensor. The flow was applied for 2.12 s, which is shorter than the duration of the experiment, but long enough for each simulation to reach a steady state after a transient period of 1.35 s or less. The transient behavior of the conformation tensor during flow is shown in Figure 4a. On the basis of this behavior, the average conformation tensor was calculated as an average over the final 0.77 s of the simulation. Because of the flow geometry, in which the sample is sheared in the x−y plane, only the *xx*, *yy*, *zz*, and *xy* components of the conformation tensor deviate from their equilibrium values, which in turn are prescribed by $\mathbf{C}_{eq} = \mathbf{I}/3$. The deviation of the relevant components of the conformation tensor from this equilibrium tensor as a function of the applied strain rate is shown in Figure 4b.

Using the information about the conformation tensor from the DSM simulations along with the kinetic results from FSC, we can determine the flow-enhancement parameter θ. Combining eqs 5 and 6, we derive the following model relationship:

$$a(\dot{\gamma}) = \left(\frac{\sum_{p=1}^{P} \nu_p \exp[\theta \sqrt{J_2(\mathbf{P}_{2,p}(\dot{\gamma}_r))}\,]}{\sum_{p=1}^{P} \nu_p \exp[\theta \sqrt{J_2(\mathbf{P}_{2,p}(\dot{\gamma}))}\,]} \right)^{1/4} \tag{8}$$

The $\sqrt{J_2(\mathbf{P}_{2,p}(\dot{\gamma}))}$ values were calculated for each shear rate from the DSM conformation tensor by using eq 1. For the

https://doi.org/10.1021/acs.jpcb.2c03460
J. Phys. Chem. B 2022, 126, 6529−6535

choice of reference strain rate used in this analysis, $\dot{\gamma}_r = 0$, eq 8 simplifies to

$$a(\dot{\gamma}) = \left(\sum_{p=1}^{P} v_p \exp[\theta \sqrt{J_2(\mathbf{P}_{2,p}(\dot{\gamma}))}\,] \right)^{-1/4} \tag{9}$$

Using a nonlinear least-squares fitting procedure, we fit the experimental values of $a(\dot{\gamma})$ to eq 9. A comparison between the fitted and experimental values is shown in Figure 5a, and the resulting fitting parameter obtained was $\theta = 75.2$. The $r_c(T,\dot{\gamma})$ data resulting from this parametrized model, shown in Figure 5b, agree well with the experimental trends across the range of temperatures and shear rates.

The parity shown in Figure 5a is an indication that eq 5, which was derived based on molecular simulation, is directly compatible with the experimental data. The value of θ is substantially larger than the value of 5.79 obtained from molecular simulations of $C_{150}H_{302}$.[28] This discrepancy is not easily attributable to the difference in chain architectures between the linear simulated system and the short-chain branched experimental one; Bustos et al. found that polyethylenes with varying chain architectures had similar acceleration in the rate of crystallization with similarly strong shear flows as quantified by a Weissenberg number (Wi) based on the weight-average relaxation time.[41] Nor can it be attributed easily to the onset of flow-induced nematic structure such as that reported previously[30] due to the relatively low Wi experienced by LLDPE A in this work; the largest strain rate corresponds to $Wi = 3$, based on the weight-averaged relaxation time. However, in this work we have not accounted for the partial relaxation of $\mathbf{P}_2$ of the melt that inevitably occurs during the cooling of the sample after preshearing, nor have we included contributions to $\mathbf{P}_2$ from the high-end tail of the molar mass distribution (Figure 1), which could not be parametrized from the available SAOS data.[22] We anticipate that the errors associated with these two simplifications at least partially compensate one another, but any residual error would subsequently be embedded in the empirically determined value of θ. More important, in our view, is the excellent correspondence between the experimental and model shift factors shown in Figure 5a, which indicates that the essential physics of the phenomena have been correctly identified.

5. SUMMARY AND CONCLUSIONS

Because of the large range of time and length scales involved in FEN, a multiscale approach is necessary to model this phenomenon effectively. In this study, such a framework has been demonstrated, wherein macroscale kinetic data from experiments is interpreted by using mesoscale calculations from a rheological model, along with correlations for crystallization kinetics derived at the nanoscale from molecular simulations. Experimentally, a recently developed protocol, in which the melt is presheared above the melting temperature, quenched, and then cyclically melted and recrystallized by using FSC to determine the crystallization rate, was found to be effective for determining the effect of flow history on the crystallization rate. Slip-link simulations of start-up flow were then used to determine how the applied shear rate led to changes in the molar mass-dependent conformation tensors, from which the corresponding Kuhn segment nematic order tensors were then obtained. Subsequently, a FEN expression derived from molecular simulation was used to relate the acceleration in crystallization kinetics to flow-induced changes in the Kuhn segment nematic order tensors.

The framework was demonstrated on an industrial-grade LLDPE, parametrizing and validating the FEN expressions for this material. This work serves to describe how the rate of crystallization depends on the state of flow. Combined with previously reported methods for describing how the rheology of an entangled polymer melt depends on the degree of crystallinity,[22] the prospect exists to obtain for the first time a complete description of the rheological behavior of a crystallizable polymer melt that captures the interdependencies of crystallization and flow.

■ ASSOCIATED CONTENT

Supporting Information

The Supporting Information is available free of charge at https://pubs.acs.org/doi/10.1021/acs.jpcb.2c03460.

Additional experimental results (DSC and micrographs) and details of the DSM model (PDF)

■ AUTHOR INFORMATION

Corresponding Author

Gregory C. Rutledge − *Massachusetts Institute of Technology, Cambridge, Massachusetts 02139, United States;* orcid.org/0000-0001-8137-1732; Email: rutledge@mit.edu

Authors

David A. Nicholson − *Massachusetts Institute of Technology, Cambridge, Massachusetts 02139, United States*

Marat Andreev − *Massachusetts Institute of Technology, Cambridge, Massachusetts 02139, United States;* orcid.org/0000-0003-2362-4177

Kenneth L. Kearns − *The Dow Chemical Company, Midland, Michigan 48642, United States;* orcid.org/0000-0001-5062-766X

Marius Chyasnavichyus − *The Dow Chemical Company, Midland, Michigan 48642, United States*

Daria Monaenkova − *The Dow Chemical Company, Midland, Michigan 48642, United States*

Jonathan Moore − *The Dow Chemical Company, Midland, Michigan 48642, United States*

Jaap den Doelder − *Dow Benelux BV, 4530 AA Terneuzen, The Netherlands; Eindhoven University of Technology, 5612 AZ Eindhoven, The Netherlands*

Complete contact information is available at: https://pubs.acs.org/10.1021/acs.jpcb.2c03460

Notes

The authors declare no competing financial interest.

■ ACKNOWLEDGMENTS

We gratefully acknowledge support from Dow through the University Partnership Initiative. The data presented in this report should not be construed as product specifications.

■ REFERENCES

(1) Peters, G. W. M.; Balzano, L.; Steenbakkers, R. J. A. In *Handbook of Polymer Crystallization*; Piorkowska, E., Rutledge, G. C., Eds.; Wiley: Hoboken, NJ, 2013; pp 399−431.

(2) Kumaraswamy, G. Crystallization of Polymers from Stressed Melts. *Journal of Macromolecular Science, Part C* **2005**, *45*, 375−397.

(3) Graham, R. S. Modelling Flow-Induced Crystallisation in Polymers. *Chem. Commun.* **2014**, *50*, 3531−45.
(4) Janeschitz-Kriegl, H. *Crystallization Modalities in Polymer Melt Processing*; Springer: Wien, 2010.
(5) Steenbakkers, R. J. A.; Peters, G. W. M. A Stretch-Based Model for Flow-Enhanced Nucleation of Polymer Melts. *J. Rheol.* **2011**, *55*, 401−433.
(6) Pantani, R.; Coccorullo, I.; Volpe, V.; Titomanlio, G. Shear-Induced Nucleation and Growth in Isotactic Polypropylene. *Macromolecules* **2010**, *43*, 9030−9038.
(7) Somani, R. H.; Yang, L.; Zhu, L.; Hsiao, B. S. Flow-Induced Shish-Kebab Precursor Structures in Entangled Polymer Melts. *Polymer* **2005**, *46*, 8587−8623.
(8) van Meerveld, J.; Peters, G. W. M.; Hütter, M. Towards a Rheological Classification of Flow Induced Crystallization Experiments of Polymer Melts. *Rheol. Acta* **2004**, *44*, 119−134.
(9) Janeschitz-Kriegl, H.; Eder, G. Basic Concepts of Structure Formation During Processing of Thermoplastic Materials. *J. Macromol. Sci., Part A* **1990**, *27*, 1733−1756.
(10) Eder, G.; Janeschitz-Kriegl, H.; Liedauer, S. Crystallization Processes in Quiescent and Moving Polymer Melts under Heat Transfer Conditions. *Prog. Polym. Sci.* **1990**, *15*, 629−714.
(11) Rhoades, A. M.; Gohn, A. M.; Seo, J.; Androsch, R.; Colby, R. H. Sensitivity of Polymer Crystallization to Shear at Low and High Supercooling of the Melt. *Macromolecules* **2018**, *51*, 2785−2795.
(12) Gohn, A. M.; Seo, J.; Ferris, T.; Venkatraman, P.; Foster, E. J.; Rhoades, A. M. Quiescent and Flow-Induced Crystallization in Polyamide 12/Cellulose Nanocrystal Composites. *Thermochim. Acta* **2019**, *677*, 99−108.
(13) Kearns, K. L.; Scherzer, J.; Chyasnavichyus, M.; Monaenkova, D.; Moore, J.; Sammler, R. L.; Fielitz, T.; Nicholson, D. A.; Andreev, M.; Rutledge, G. C. Measuring Flow-Induced Crystallization Kinetics of Polyethylene after Processing. *Macromolecules* **2021**, *54*, 2101−2112.
(14) Koscher, E.; Fulchiron, R. Influence of Shear on Polypropylene Crystallization: Morphology Development and Kinetics. *Polymer* **2002**, *43*, 6931−6942.
(15) Doufas, A. K.; McHugh, A. J.; Miller, C. Simulation of Melt Spinning Including Flow-Induced Crystallization: Part I., Model Development and Predictions. *J. Non-Newtonian Fluid Mech.* **2000**, *92*, 27−66.
(16) Zuidema, H.; Peters, G. W. M.; Meijer, H. E. H. Development and Validation of a Recoverable Strain-Based Model for Flow-Induced Crystallization of Polymers. *Macromol. Theory Simul.* **2001**, *10*, 447−460.
(17) Coppola, S.; Grizzuti, N.; Maffettone, P. L. Microrheological Modeling of Flow-Induced Crystallization. *Macromolecules* **2001**, *34*, 5030−5036.
(18) Graham, R. S.; Olmsted, P. D. Coarse-Grained Simulations of Flow-Induced Nucleation in Semicrystalline Polymers. *Phys. Rev. Lett.* **2009**, *103*, 115702.
(19) Read, D. J.; McIlroy, C.; Das, C.; Harlen, O. G.; Graham, R. S. Polystrand Model of Flow-Induced Nucleation in Polymers. *Phys. Rev. Lett.* **2020**, *124*, 147802.
(20) Schieber, J. D.; Neergaard, J.; Gupta, S. A Full-Chain, Temporary Network Model with Sliplinks, Chain-Length Fluctuations, Chain Connectivity and Chain Stretching. *J. Rheol.* **2003**, *47*, 213−233.
(21) Andreev, M.; Rutledge, G. C. A Slip-Link Model for Rheology of Entangled Polymer Melts with Crystallization. *J. Rheol.* **2020**, *64*, 213−222.
(22) Andreev, M.; Nicholson, D. A.; Kotula, A.; Moore, J. D.; den Doelder, J.; Rutledge, G. C. Rheology of Crystallizing LLDPE. *J. Rheol.* **2020**, *64*, 1379−1389.
(23) Andreev, M.; Khaliullin, R. N.; Steenbakkers, R. J. A.; Schieber, J. D. Approximations of the Discrete Slip-Link Model and Their Effect on Nonlinear Rheology Predictions. *J. Rheol.* **2013**, *57*, 535−557.
(24) Khaliullin, R. N.; Schieber, J. D. Application of the Slip-Link Model to Bidisperse Systems. *Macromolecules* **2010**, *43*, 6202−6212.
(25) Pilyugina, E.; Andreev, M.; Schieber, J. D. Dielectric Relaxation as an Independent Examination of Relaxation Mechanisms in Entangled Polymers Using the Discrete Slip-Link Model. *Macromolecules* **2012**, *45*, 5728−5743.
(26) Rutledge, G. C. In *Handbook of Polymer Crystallization*; Piorkowska, E.; Rutledge, G. C., Eds.; Wiley: Hoboken, NJ, 2013; pp 197−214.
(27) Graham, R. S. Understanding Flow-Induced Crystallization in Polymers: A Perspective on the Role of Molecular Simulations. *J. Rheol.* **2019**, *63*, 203−214.
(28) Nicholson, D. A.; Rutledge, G. C. An Assessment of Models for Flow-Enhanced Nucleation in an n-Alkane Melt by Molecular Simulation. *J. Rheol.* **2019**, *63*, 465−475.
(29) Anwar, J.; Zahn, D. Uncovering Molecular Processes in Crystal Nucleation and Growth by Using Molecular Simulation. *Angew. Chem., Int. Ed.* **2011**, *50*, 1996−2013.
(30) Nicholson, D. A.; Rutledge, G. C. Flow-Induced Inhomogeneity and Enhanced Nucleation in a Long Alkane Melt. *Polymer* **2020**, *200*, 122605.
(31) Kuhn, W.; Grün, F. Beziehungen Zwischen Elastischen Konstanten Und Dehnungsdoppelbrechung Hochelastischer Stoffe. *Kolloid-Z.* **1942**, *101*, 248−271.
(32) Fuller, G. G. *Optical Rheometry of Complex Fluids*; Oxford University Press: New York, 1995.
(33) Cassagnau, P.; Montfort, J. P.; Marin, G.; Monge, P. Rheology of Polydisperse Polymers: Relationship between Intermolecular Interactions and Molecular Weight Distribution. *Rheol. Acta* **1993**, *32*, 156−167.
(34) Fetters, L. J.; Lohse, D. J.; Richter, D.; Witten, T. A.; Zirkel, A. Connection between Polymer Molecular Weight, Density, Chain Dimensions, and Melt Viscoelastic Properties. *Macromolecules* **1994**, *27*, 4639−4647.
(35) Stephanou, P. S.; Baig, C.; Tsolou, G.; Mavrantzas, V. G.; Kröger, M. Quantifying Chain Reptation in Entangled Polymer Melts: Topological and Dynamical Mapping of Atomistic Simulation Results onto the Tube Model. *J. Chem. Phys.* **2010**, *132*, 124904−124904.
(36) Everaers, R.; Sukumaran, S. K.; Grest, G. S.; Svaneborg, C.; Sivasubramanian, A.; Kremer, K. Rheology and Microscopic Topology of Entangled Polymeric Liquids. *Science* **2004**, *303*, 823−6.
(37) Rubinstein, M.; Colby, R. H. *Polymer Physics*; Oxford University Press: Oxford, 2003.
(38) Schieber, J. D.; Andreev, M. Entangled Polymer Dynamics in Equilibrium and Flow Modeled through Slip Links. *Annu. Rev. Chem. Biomol. Eng.* **2014**, *5*, 367−381.
(39) Valadez-Pérez, N. E.; Taletskiy, K.; Schieber, J. D.; Shivokhin, M. Efficient Determination of Slip-Link Parameters from Broadly Polydisperse Linear Melts. *Polymers (Basel)* **2018**, *10*.908.
(40) Ergoz, E.; Fatou, J. G.; Mandelkern, L. Molecular Weight Dependence of the Crystallization Kinetics of Linear Polyethylene. I., Experimental Results. *Macromolecules* **1972**, *5*, 147−157.
(41) Bustos, F.; Cassagnau, P.; Fulchiron, R. Effect of Molecular Architecture on Quiescent and Shear-Induced Crystallization of Polyethylene. *J. Polym. Sci., Part B: Polym. Phys.* **2006**, *44*, 1597−1607.

https://doi.org/10.1021/acs.jpcb.2c03460
J. Phys. Chem. B 2022, 126, 6529−6535